Mechatronic Design and Control of a Robotised Crane Exploiting Natural Dynamics for Pick-and-Place Applications

Boris Deroo[1,†], Erwin Aertbeliën[1,2], Wilm Decré[1,2], and Herman Bruyninckx[1,2,3]

***Abstract*—This paper describes a solution for pick-and-place tasks that do not require high precision throughout the execution, using a robotised gantry crane. Two common issues that occur when using a crane are addressed, and solutions are provided.**

First, the lack of rotational controllability is overcome by designing a gripper that passively aligns itself with the handle of the payload using a simple, robust control strategy. Second, the active workspace is expanded by using controlled, dynamic motions, based on a variable-length pendulum model. Thus, the workspace is no longer limited to positions directly accessible from above, as is the case with quasi-static control methods. The robustness and effectiveness of the proposed solution was validated by a grasping, and a shelf insertion experiment.

The robot was able to grasp the payload during all 48 trials. Failures were detected and recovery strategies were implemented. The handle could also be reliably ungrasped. During the shelf insertion, imperfect trajectory tracking caused a significant error during the unobservable part of the trajectory. Nevertheless, the actual placement position was always close to the desired position.

***Index Terms*—Industrial robots, grasping, dynamics, underactuated robots.**

I. Introduction

IN the **context** of construction applications, cranes are dominant for pick-and-place task of heavy payloads. Despite the cranes' inherent flexibility and underactuated nature, skilled crane operators are able to precisely control and position payloads. A complementary, common control approach is to have an operator on the ground directly control the end-effector in parallel with the crane operator to achieve the task precision (Fig. 1). In robotic terms, the task is separated between multiple heterogeneous agents with different subtasks: the heavy but imprecise macro-movement; and the light but accurate micro-placement. Interactions with the environment are exploited to work faster, more precisely, and to reduce physical effort. For example, using a previously placed brick to guide the brick that is currently being placed; bracing against said brick to mechanically line them up; sliding instead of fully lifting; or making contact to quickly dampen out oscillations.

This interaction-based approach can especially be exploited for 'rough' pick-and-place applications. In this work these are defined as applications where precision is only required at the beginning, and/or end of the task, but do not require strict trajectory-tracking during the majority of the free-space motion. The payload is not fragile, and (controlled) collisions with the environment are not detrimental for a successful task completion. There are plenty of other examples of such applications outside of the construction industry, especially in the logistics industry: (de)palletising, truck (un)loading, moving objects on (or across) conveyor belts, etc. The mechatronic design methodology followed by the robotics sector for such tasks is however drastically different compared to humans performing these same tasks.

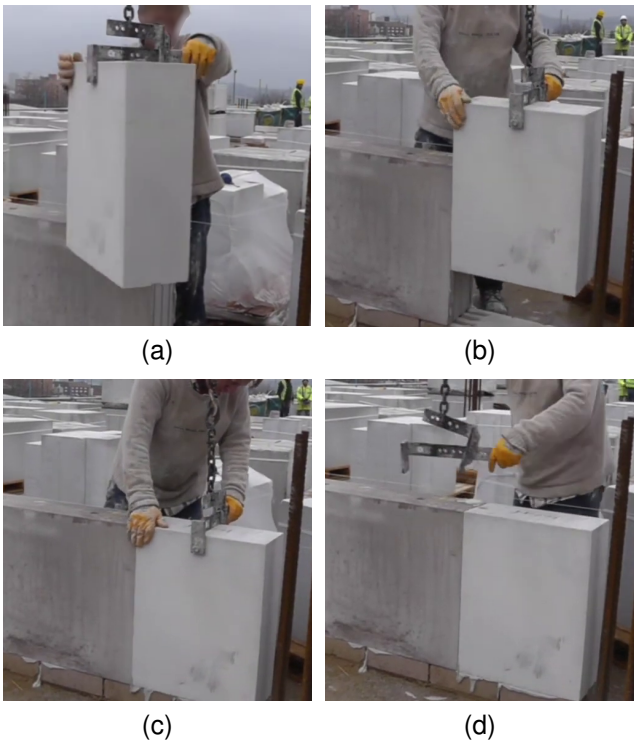

Fig. 1. Ground operator controlling a payload in parallel with a crane operator to construct a wall [1]. (a) Guiding the payload into position. (b) Colliding with the environment to achieve precision. (c) Making contact with the ground. (d) Ungrasping the end-effector.

The **current** push for automation in these applications consists of generic, all-purpose serial robots. These robots typically have between five to seven degrees of freedom (DoF), which provide ample flexibility for a wide range of operations. The control approach is based on accurately following pre-programmed trajectories in space with its end-effector, or the interaction dynamics are realised actively by a form of *admittance* or *impedance control* [2]. This is opposed to the dynamic- and interaction-based approach mentioned above. Stiff links are required for this control approach since it relies on the inverse kinematics of rigid bodies. The weight of the robot scales approximately linearly with respect to the rated payload when designing for stiffness [3] (comparing

[1] Department of Mechanical Engineering , KU Leuven, 3000 Leuven, Belgium `first_name.second_name@kuleuven.be`
[2] Flanders Make, 3000 Leuven, Belgium
[3] Department of Mechanical Engineering, TU Eindhoven, Eindhoven, The Netherlands
† Corresponding author

the models with the highest rated payload to weight ratio of each series). This results in heavier robots for higher payloads, and consequently costly, energy-inefficient, and mechanically unsafe solutions.

Human control and trajectory-based robot control also differ significantly in the use of motions following the natural dynamics for 'rough' pick-and-place tasks (Fig. 2). Instead of fully controlling and constraining the path of the payload, the payload follows the natural dynamic motion depending on its current state. Timely adding or removing motion constraints can still influence this motion in order to guide the payload towards the desired position. Such motions require less input energy than trajectory-based motions, but their duration is not controllable.



Fig. 2. Human moving with the natural dynamics of the payload during truck unloading [4]. (a) Grabbing the payload, (b) Carrying the payload towards a starting position for the natural dynamics. (c) Guiding the payload while it is falling. (d) Placing the payload on its target position.

Three levels of increasing difficulty are categorised for robots performing tasks using such dynamic motions. To this end, the concept of the static workspace is defined as: positions in which the robot can hold the payload in place indefinitely.

1) Dynamic motions can occur completely within the static workspace to reach an end position faster. The system remains controllable and observable. At the end of the dynamic motion, linear feedback control can still be used to compensate errors of the end-position.
2) Dynamic motions can be performed to reach a position outside of the static workspace, where the system is observable during the whole motion. While errors can be perceived, the system is no longer fully controllable throughout the motion. Thus, it might not be possible to compensate these errors with feedback control.
3) Dynamic motions can be performed to reach a position outside of the static workspace, where the system is non-observable during (sections of) the motion. The system is no longer fully controllable, nor fully observable. During these sections, potential errors can not be monitored.

This work presents an alternative, partly passively controlled, distributed **solution** for 'rough' pick-and-place applications. It is inspired by the approach utilised by humans, instead of the traditional path-following approach. By relaxing the stiffness requirement necessary for the inverse kinematic control, lighter robot structures can be used, resulting in a more cost-effective, and safe solution.

The requirements for the 'rough' pick-and-place applications are taken as the starting point for the mechatronic solution. The focus lies on co-developing the mechanics, the used models, and the control approach within the context of the task, instead of developing just a single one of these aspects. It is attempted to minimise the moving mass (and thus the safety in case of collisions with humans or the environment, and the energy consumption during operation), and develop a solution that is complementary with respect to other mechatronic agents.

These agents are responsible for different subtasks of the application, and are designed for their respective subtask-specific requirements. For the 'rough' pick-and-place applications, a first (complementary) separation of the task specification can be made between: a robot responsible for the heavy, macro-movement; and a robot responsible for the accurate, micro-placement. This would be analogue to the strategy employed in the construction industry, with crane- and ground operators.

While working towards a multi-agent, task-specific solution, this paper presents the result for the macro-movement of the task execution. To this end, a robotic gantry crane was built. Compared to serial robots, gantry systems and cranes scale better with the workspace relative to the moving mass and energy consumption. This is in part due to the decoupling of the actuated axes that manipulate the gravitational and inertial directions. A secondary effect of this decoupling is that the movement is also more predictable and interpretable for human bystanders, inherently improving the safety as well. Due to the hoisting cable, the moving mass of the robot is low and the payload is inherently compliant, except in the downward direction of the cable. Thus, in case of a collision, only the energy of the payload, and not the robot, will be instantaneously transferred to the objects with which it collides. The gears of the motor will also not feel the direct impact of the collision. This improves the safety for both the colliding object (or human), and the robot itself.

However, a **shortcoming** of a gantry crane is that it can only control the three positional DoF of the payload and is underactuated in the three orientation DoF. While this saves on additional actuation, it does drastically limit the functionalities compared to a serial structure. Grasping an object with a certain orientation is especially difficult. Another downside of a gantry crane is that its workspace is typically limited to positions that are only directly accessible from above. This is because generally a quasi-static control approach is used, in order to limit the sway of the payload.

These shortcomings of gantry cranes are addressed by two complementary **contributions**:

First, the gripper hardware is co-designed with the task to mechanically control the orientation when performing a grasp-

ing motion. This allows the underactuated system to reliably grasp a payload, regardless of its position and orientation, using only simple low-level controllers.

Secondly, a control strategy is proposed that makes use of the system's natural dynamics, allowing for payloads to be placed outside of the static workspace.

The continuous controllers used in the different parts of the execution are coordinated by a discrete controller that is implemented as a finite state machine (FSM). Monitors are used to track the nominal behaviour of the execution during the different states. This allows the system to detect failures during certain substates, automatically resetting, and retrying the execution if possible, hence providing robustness to the approach.

The approach will be **validated** by performing a shelf insertion experiment, where a crate payload is inserted horizontally in a position that is obstructed from above. This corresponds to a dynamic motion of the most difficult level as explained earlier. A variable-length pendulum model is used to model the dynamic behaviour of the end-effector.

The **expected impact** of this paper is to show that by developing/improving some aspects of the hardware, model, and controller together, even a simple, cheap gantry system can be used to perform a complex task that it would not be able to do if a quasi-static control approach was used. A single camera is used as the only external sensor to provide direct end-effector position sensing, through simple colour detection algorithms, to the robot set-up. This shows the limited sensing required for the proposed approach to perform the task.

To summarise, the objective of this work is to perform a commonly occurring task, with a minimal amount of actuators, in order to save both component and energy costs. The constraint is that the underactuated system cannot directly control all the required DoF. The trade-off of the proposed approach is that energy needs to be stored in the system before executing the trajectory, and during certain stages of the execution there is less or no controllability (of the exact followed path and timing) and/or observability.

The rest of the paper is organised as follows: The related literature is presented in Sec. II. The experimental set-up is introduced in Sec. III. The pendulum model used for the shelf insertion is given in Sec. IV. The design of the gripper that is able to passively align itself with a crate handle is discussed in Sec. V. The task execution for the validation use case to grasp and shelf a crate is explained in Sec. VI. The experimental validation of the use case, and the discussion of the results are detailed in Sec. VII. Final conclusions about these results are made in Sec. VIII. Lastly, the text is concluded with future work in Sec. IX.

II. Related Literature

A. Anti-Sway Control of Cranes

Most research covering the control of crane systems are focused on reducing and eliminating the (in most applications unwanted) swaying of the payload. One way of achieving this behaviour is by shaping the root locus of the dynamic system in the control loop [5]. Other common feedback methods include fuzzy control [6], and sliding mode control [7].

Another approach is to apply feedforward inputs that limit the sway. Input shaping techniques modify the input command such that the excited harmonic modes cancel each other out after the input command is finished [8]–[10]. However, input shaping can also be used to amplify the sway of the payload, in order to store more energy in the swinging payload [11].

The swaying of the payload will be similarly exploited in this work to store energy, in order to reach end states that would not be reachable with a (quasi-)static approach.

B. Use of Environment for Control

For cable-driven parallel robots (CDPR), the control approach cannot handle interactions with the environment of the links (cables), drastically limiting the workspace in cluttered environments. Cable-object collisions are unwanted and thus avoided. One proposed solution to operate CDPRs in obstacle dense environments is to combine a serial manipulator at the end-effector of the CDPR [12]. The CDPR is responsible for the macro-movement. Whereas the manipulator is used for the micro-movement, to reach positions obstructed by obstacles. The approach laid out in this paper instead exploits interactions of both the end-effector and the cable to reach positions that are obstructed.

Mason has previously established primitives to describe the mechanics of pushing [13]. The concept of the friction cone and centre can be used to describe how an object on a surface will move when pushed. In this work, an end-effector is suspended by a cable from a gantry, and will interact with its environment. This can be seen as a simplified version, with the environment providing pushing forces to the end-effector (depending on the inclination angle of the cable). The anchor point can be seen as the centre of friction, as the end-effector moves without friction forces through free space.

The environment can also be used to assist in gripping [14]. It acts as a constraint that guides the gripper towards stable grasps. Compliant hardware that complements this strategy allows for simpler controllers, and no explicit force sensing or feedback, as is necessary with rigid grippers.

C. Trajectory Tracking

When tracking a specified trajectory, it is attempted at every time-instance to have the robot at a prespecified state. In the work of Swevers et al., model predictive control (MPC) and optimal control has been used extensively to shape the trajectory of a robot given a dynamic model and constraints [15]–[18]. An optimisation is performed to calculate the required control inputs at every time step, based on the current state, and the predicted future states.

Depending on the objective, different aspects can be optimised, such as the total execution time, or the energy consumption, resulting in different trajectories [19]. For robots with actuator redundancies, this redundancy can be exploited to generate more energy-efficient trajectories at the joint level [20]. Given a specific path, time-scaling the trajectory can also reduce the energy consumption [21]

In our previous work, a control approach was used that stepped back from trajectory tracking. It focused instead on

reaching only certain key positions of the task execution that are of interest (e.g. the end position). The methodology made direct use of the natural dynamics of the system, redundancy in the actuation to influence these dynamics, and interactions with the environment [22], [23]. It was shown that this could drastically lower the energy consumption of the execution, and that even with imprecise hardware, the task could accurately be completed.

D. Out-of-Static-Workspace Control

Most control approaches for robots only operate in the static workspace. Thus, the time-dependency of the trajectory can be controlled by changing the execution speed. Ballistic motions, where the payload is thrown, are trajectories where the timing cannot be independently controlled. They have been studied extensive in robotic research [24]–[26].

For low velocities, gravity is the only dominant external force during the airbourne phase. The ballistic trajectory is solely determined by the state of the payload when it leaves the end-effector of the robot. While the underlying physical models are simple, the payload losses all controllability after it has been thrown, limiting the achievable end-states and applications. Some robot designs overcome this limitation by maintaining a physical connection (such as a cable) with the payload, to influence the trajectory of the payload even after it has been thrown.

The 'casting manipulator', developed by Arisumi et al., connects a rigid link to the payload by a string similar to a fishing reel [27], [28]. A brake provides discrete braking actions to the string. The rigid link swings the end-effector, which is launched by releasing the brake. However, the trajectory can still be influenced by selectively braking the string, providing impulse forces to the end-effector. This allows the end-effector to reach arbitrary positions and significantly improves the workspace. It also uses substantially less energy compared to a robot with larger links, or a mobile base.

The 'winch-bot' is an underactuated 2-DoF robot consisting of a single actuator connected to a winch capable of moving in the vertical plane [29], [30]. First, energy is injected in the system by self-excitation. Afterwards this energy can be manipulated by controlling the speed of the winch. A similar underactuated robot, which is also capable of controlling the orientation of the end-effector in the vertical plane using two actuators, was designed in [31]. Using feedback linearisation, the dynamics can be decoupled into a variable-length pendulum system, and a system that controls the end-effector orientation. These works show that generic trajectories can be followed with an underactuated system, by sacrificing control over the execution speed. Other examples of underactuated systems used to perform point-to-point motions in the vertical plane outside of the static workspace are given in [32], [33].

This paper uses similar concepts for the 'rough' pick-and-place operation.

III. Experimental Set-up

To experimentally validate the proposed approach, the low-cost set-up depicted in Fig. 3 was built. It consists of a ceiling-mounted gantry system, which allows for movements in the horizontal plane [34]. It uses stepper motors with 2Nm holding torque to move over a workspace of 100cm by 50cm. Attached to the gantry's end-effector is a brushless DC motor, which acts as a hoist. It has a rated power of 66W and a rated torque of 0.58Nm. The motor shaft is attached to a gear transmission of $\frac{80}{21}$, which is connected to a drum with a radius of 5.4cm. The anchor point of the hoist cable is positioned 2.68m above the ground. The shaft of the hoist is attached to a drum with a diameter of 11cm. Because of its high strength and low elasticity, Dyneema rope [35] is used to connect the gripper to the drum. All actuators have encoders at their outputs. The gantry frame is rated for a maximum payload of $\pm$10kg.

The specific methodology described in this work is also fully compatible with other overhead-planar robots, e.g. [36].

The beer crate displayed in Fig. 3 was used as the payload for both the grasping and insertion task as will be explained in Sec. VI.

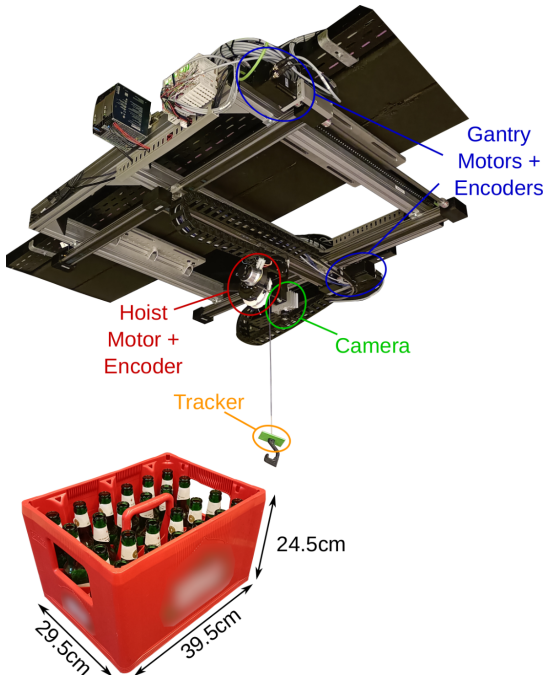

Fig. 3. Set-up and crate that were used for the grasping and shelf insertion validation experiments. The robot consists of a hoist motor attached to a gantry system that is mounted to the ceiling, allowing control in 3 DoF.

A Basler 160 frames-per-second camera (a2A1920-165g5cBAS) with a 4mm focal length lens is connected to the hoist. It points straight down, providing a top-down image of the scene. This image is used to detect both the position of the tracker, attached at the end of the cable above the gripper, and the crate that will be manipulated. Both are detected based on straightforward colour detection algorithms. Figure 4 provides a frame as seen by the camera.

The task control output is the end-effector pose. This is estimated based on the position-tracker in the camera frame, and the hoist length l. The end-effector is only partially observable and controllable, since its rotation along the cable cannot be observed, nor controlled. The task control input (and the robot control output) is the velocity $\dot{l}$ of the hoist, and the

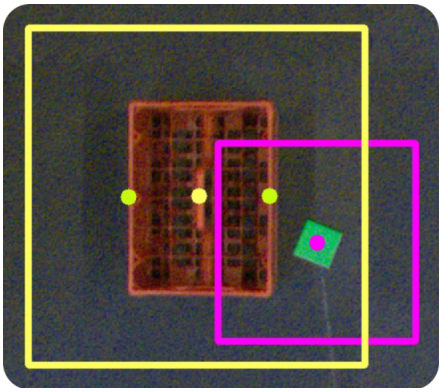

Fig. 4. Image frame provided by the camera. The searched region of interest for the end-effector, and its detected position is depicted in magenta. The region of interest for the crate, and certain of its positions of interest (as will be explained in Sec. VI-A) are depicted in yellow.

position of the gantry bed. Since the dynamics of the hoist motor controller are magnitudes faster than the dynamics of the swinging crane, it is assumed that the motor can instantly track the velocity input $\dot{l}$.

IV. Pendulum Model

In this work, the shelf insertion (as will be discussed in Sec. VI-B) is modelled as a motion in the 2D vertical plane. This assumption is made since the out-of-plane direction is never excited during the execution: not when the payload is moved in the 3D workspace before the dynamic motion (since this occurs quasi-static); nor during the dynamic motion itself (since this motion occurs solely in the vertical plane). In case the dynamic motion is excited in the 3D space, the model should be augmented to take this extra dimension into account. However, this is considered unnecessary to illustrate the core concepts that are the focus of this paper.

Following assumptions are also made:

1. The payload can be treated as a point mass.
2. The cables are massless and infinitely stiff in the axial direction.
3. Aerodynamic effects can be neglected.
4. When the cable slides over the edge of the shelf, the friction can be neglected.
5. The default factory velocity controller of the hoist motor drive can track the velocity input sufficiently fast.

A. Variable-Length Pendulum Model

The dynamic equations of a variable-length pendulum can be constructed using the Euler-Lagrange approach:

$$\begin{aligned} T &= \frac{1}{2}m((\dot{\theta}l)^2 + \dot{l}^2), \\ V &= -lgm\cos(\theta), \\ L &= T - V, \\ \frac{d}{dt}(\frac{\partial L}{\partial \dot{\mathbf{p}}}) - \frac{\partial L}{\partial \mathbf{p}} &= \mathbf{u}, \\ \mathbf{p} &= [\theta, l]^\top, \\ \mathbf{u} &= [0, -F]^\top, \end{aligned} \tag{1}$$

with the geometric parameters as specified in Fig. 5, T and V respectively the kinetic and potential energy, m the mass of the payload, g the gravitational acceleration, and F the cable tension force. This results in following dynamic equations of motion in the tangential and radial directions respectively:

$$\ddot{\theta} = -2\frac{\dot{l}\dot{\theta}}{l} - g\frac{\sin(\theta)}{l}, \tag{2a}$$

$$\frac{F}{m} = -\ddot{l} + \dot{\theta}^2 l + g\cos(\theta). \tag{2b}$$

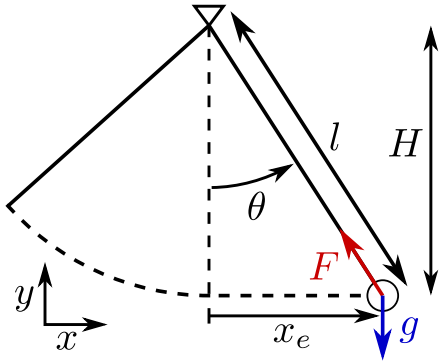

Fig. 5. Variable-length pendulum with the end-effector moving along a straight line after reaching the bottom-most position.

Equation (2b) can be used to validate that there is no cable slack, by monitoring whether F remains positive, i.e. the change in cable speed should be limited by:

$$\ddot{l} \leq g\cos(\theta) + \dot{\theta}^2 l. \tag{3}$$

By controlling the unwinding speed of the hoist $\dot{l}$, the end-effector can track specific trajectories in the vertical plane. Due to the underactuated nature of the planar motion of the pendulum, the reachable positions are time- and state-dependent, governed by (2a) and (3).

In the case of moving along a straight line (with ϕ the angle w.r.t the x-axis), following analytic solution can be derived:

$$\tan(\phi) = \frac{\dot{\theta}l\sin(\theta) - \dot{l}\cos(\theta)}{\dot{\theta}l\cos(\theta) + \dot{l}\sin(\theta)}. \tag{4}$$

Or in the specific case of moving horizontally ($\phi = 0$):

$$\dot{l} = \dot{\theta}l\tan(\theta). \tag{5}$$

The work W done in the radial direction during this motion can be obtained by integration over a time horizon T:

$$W(T) = \int_0^T F\dot{l}\mathrm{d}t. \tag{6}$$

For the special case when the end-effector moves along a straight line, an analytical solution can be found by integrating the horizontal cable force component F_X over the total travelled horizontal distance x_{tot} [29].

$$F_X(x) = -mg\tan(\theta) = -mg\frac{x}{H}, \tag{7}$$

$$W(x_{tot}) = \int_0^{x_{tot}} F_X\mathrm{d}x = -\frac{mg}{2H}x_{tot}^2. \tag{8}$$

B. Two-Phase Pendulum Model

By swinging the end-effector, certain positions can be reached that are vertically obstructed from above (e.g., shelves). The cable will make contact with the top of the shelf during the swing if the swing amplitude is large enough, as illustrated in Fig. 6. Thus, a two-phase variable-length pendulum model can be used.

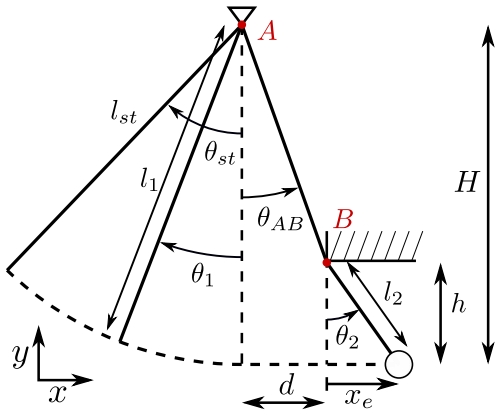

Fig. 6. Two-phase pendulum motion, starting with zero end-effector velocity at l_{st} and θ_{st}. The cable will touch the corner of the shelf at position B after reaching $\theta_1 = \theta_{AB}$. This results in a second pendulum motion with B as pivot point. When $\theta_1 \geq 0$, the pendulum moves horizontally to perform an insertion motion.

It is assumed that the pivot point B is infinitely stiff, and that the friction between the cable and the corner (point B) is negligible compared to the inertial force at the end-effector. Thus, it is assumed that the cable slips smoothly over the corner without slacking. The second phase of this model corresponds to a discrete change of the pivot point (from point A to point B in Fig. 6) when $\theta_1 = \theta_{AB}$. At this instance, the model parameters change as follows:

$$\theta_1 = \theta_2 = \theta_{AB}, \tag{9a}$$

$$l_2 = l_1 - |AB|, \tag{9b}$$

$$\dot{\theta}_2 = \dot{\theta}_1 \frac{l_1}{l_2}, \tag{9c}$$

and $\ddot{\theta}_2$ as given by (2a).

The velocity v of the end-effector during the horizontal part of the trajectory ($\theta \geq 0$) can be derived from the (kinetic) energy E present in the system. This energy can be obtained by subtracting the work done by the hoist, from the starting total (potential) energy E_{st}.

For the specific case where the cable length is first held constant at $l_{st} = H$, and a horizontal trajectory is desired when the end-effector reaches its lowest position (Fig. 6):

$$E_{st} = mgH(1 - \cos(\theta_{st})), \tag{10}$$

$$E = \frac{mv^2}{2} = E_{st} + W_d + W_{x_e}, \tag{11}$$

with W_d and W_{x_e} the work done over the distance d and x_e (see Fig. 6) respectively. Using (8), this can be written as a function of the end-effector velocity:

$$v = \sqrt{g\left(2H\left(1 - \cos(\theta_{st})\right) - \frac{d^2}{H-h} - \frac{x_e^2}{h}\right)}. \tag{12}$$

The maximum insertion distance $x_{e,\max}$ is reached when v becomes zero and is given by:

$$x_{e,\max} = \sqrt{h\left(2H\left(1 - \cos\left(\theta_{st}\right)\right) - \frac{d^2}{H-h}\right)}. \tag{13}$$

As can be seen from (13), $x_{e,max}$ is largest when $d = 0$, or i.e. the cable anchor point of the gantry is directly over the top corner of the shelf.

V. Gripper Design

This section deals with the design of a passive gripper for grasping a payload. The design makes use of unstable surfaces to passively self-align itself. This results in a predictable behaviour when it is in contact with the payload to be grasped. The design of this gripper is complementary to the control approach used. In this work, a design is made for grasping a payload with a handle (more specifically, the beer crate depicted in Fig. 3). However, the principles discussed can be translated to other methods to grasp a payload as well.

In this paper a handle is defined as: A part of an object with a cross section that is a magnitude smaller than its length; This cross section can be approximated as a rectangle or ellipse; The handle is locally free along its length, providing access from all directions. Handles can be grasped by a hook, as is often used with gantry systems for hoisting. Similarly, this work will focus on the design of a hook-shaped gripper.

Following assumptions are made for the grasping execution:

1. Aligning the gripper can be modelled as quasi-static in the 2D horizontal plane.
2. The energy of the gripper will dissipate over time when it collides with the handle.
3. The position of the gripper and the handle are known in the world frame.
4. The height of the gripper can be sufficiently accurately controlled, such that the height of the handle is entirely within Ω (as defined in Fig. 8).

A. Control through Mechanics

A gantry system is underactuated in the three rotational DoF of the end-effector. When the system is (quasi-)statically used, the centre of mass of the gripper is in the extension of the cable. Thus, two of the rotational DoF are in a predictable, determined state. Only the DoF along the axis in line with the cable, the yaw of the gripper, is unknown and undetermined. Making the gripper contact the handle is trivial with a 3 DoF system like a gantry, controlling the yaw to align with the handle is less trivial.

However, the surface of the gripper can be designed such that it is self-aligning given a force in the horizontal plane F_G provided by the gantry (Fig. 7). This exploits the fact that the gripper can freely rotate around its yaw axis to make its behaviour predictable. Thus, the gripper is indirectly controlled through its mechanics by the gantry.

This concept also works for other robot structures, and rotational axes, provided that the gripper is connected with a revolute joint that allows it to freely rotate around the axis of interest.

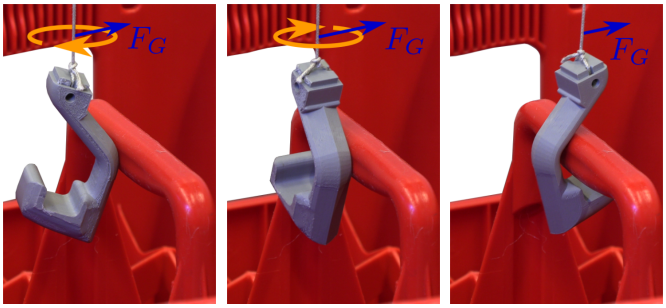

Fig. 7. By designing the surface of the gripper, a specific end-orientation can be mechanically achieved due to an external force in the horizontal plane F_G provided by the underactuated crane (a video execution is shown in [37]).

B. Crate Grasping Gripper

The gripper designed to grasp the handle of a payload, and the corresponding design parameters, are depicted in Fig. 8.

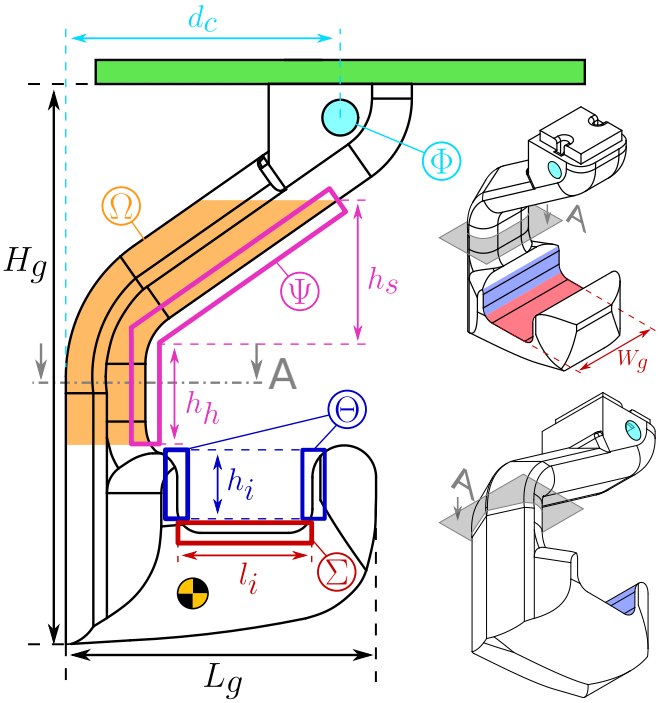

Fig. 8. Gripper design. The camera tracker is shown in green (it is omitted in the perspective views for clarity). The cable attachment hole is indicated with Φ. The shaft of the gripper is marked with Ω. The front of the gripping area is highlighted with Ψ. The inner gripping area consists of Θ and Σ. The centre of gravity (CoG) is depicted with a yellow-black circle.

The hoist cable of the robot is connected to the gripper through Φ. The shaft of the gripper (Ω) is designed to make contact with the handle during the alignment. The vertical position of the handle should be completely within this area when the gripper approaches it. Thus, h_s and h_h should be chosen such that h_s+h_h is larger than the height of the handle. A margin can be added to allow a tolerance on the required height of the gripper when approaching the handle, and as such make it more robust against disturbances of this height. This will however make the gripper taller, causing it to be less manoeuvrable.

Independent of the exact position on Ω the handle makes contact with, the gripper will align itself with the handle (see Sec. V-C). This causes the handle to end up in contact with the front of the gripping area (Ψ). The distance from the cable attachment point to all possible contact positions d_c should be sufficiently large in order to guarantee that the gripper is always able to align itself (Sec. V-C). But again, a larger d_c will make the gripper less manoeuvrable.

The area h_s is slanted such that the gripper will slide over the handle when it is moved closer towards the handle, guiding it to h_h. By reeling in the hoist cable, the gripper will be lifted, causing the handle to slide into the inner gripping area (Σ and Θ).

The inner gripping area is designed to fit closely around the handle to provide a secure grasp. Thus, l_i should be close to the width of the handle. The larger width W_g of the inner gripping area ensures a stable grasp due to the additional friction area. This makes the payload less prone to sliding along the gripper, and tipping if the grasp is not centered enough.

The inner gripping area could be made more suitable for generic handle shapes by having a v-shaped cross-section (Fig. 9a). Similarly, in case of a non-uniform shape along the length of the handle (e.g. a more human-ergonomic convex shape), a two-pronged gripping area could be used (Fig. 9b). However, in this work the overconstrained grasp was chosen since it provides more robustness. More specific designs could also be easily manufactured with the used 3D-printing method.

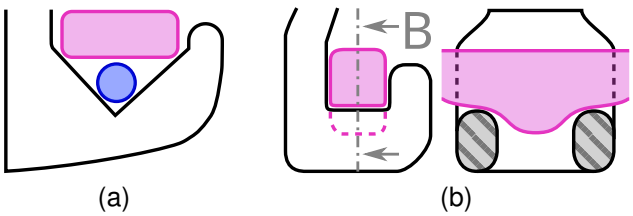

Fig. 9. Inner gripping area alternatives to hold different handle shapes. (a) Side view of a V-shaped inner gripping area, with a rectangular and circular handle cross-section. (b) Side view, and cross-section of the front view of a fork-shaped inner gripping area, for a non-uniform handle.

The remaining geometric parameters (H_g and L_g) should be chosen such that the gripper is small enough to efficiently manoeuvre and rotate around the handle of the payload without getting stuck, while at the same time making sure the gripper remains strong enough to be able to lift the payload.

For the specific application of grasping beer crates, the bottom of the gripper is wedge-shaped, such that when it is lowered into the crate, it cannot rest upright on a bottle, and will topple over. This will cause it to fall in between the bottles, and hence it will not get stuck.

C. Gripper Aligning Mechanism

In the anticipated scenario, the gantry moves perpendicular to the handle. The gripper will however not necessarily collide frontally with the handle, and might need to be reoriented in the 2D-horizontal plane. This self-orienting of the yaw angle is illustrated with a quasi-static model in Fig. 10. The gripper starts in contact with the handle, but with a possible wrong

orientation. By moving the gantry in the general direction of the handle, the reaction force of the handle F_R (due to the cable force in the horizontal plane F_G), will cause the gripper to rotate towards the desired configuration. By designing the distance d_c (between the cable attachment point, to the point of the gripper currently in contact with the handle) to be longer, the lever arm of the moment will be larger, causing the gripper to rotate more easily.

If F_R is within the green area depicted in Fig. 10b, the gripper is dynamically unstable and it will rotate towards the desired configuration due to the induced moment. Only the desired configuration corresponds to a stable equilibrium.

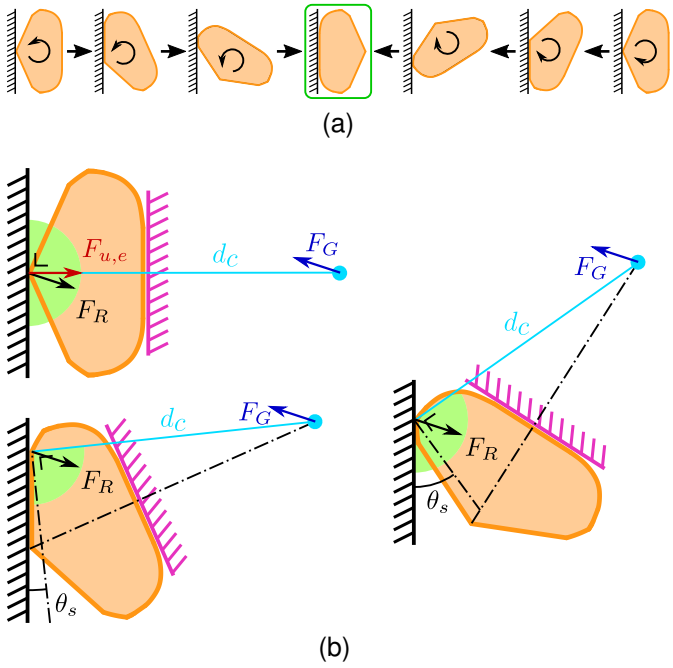

Fig. 10. Top-down view of cross-sections of the gripper (section view A of Fig. 8), during the alignment process. The gripper is given in orange, the handle in black. (a) Aligning the gripper to the desired stable configuration (green highlight). (b) Force diagram for different gripper configurations. The desired handle position is given in magenta. The cable attachment point is indicated by ● and is positioned above the displayed cross-sections. F_G and F_R are the cable force in the horizontal plane, and the reaction force respectively. $F_{u,e}$ is the force corresponding to an unstable equilibrium point.

As long as all points of the gripper surface currently in contact with the handle lie to the same side of the cable force in the horizontal plane F_G, a rotating moment will be induced. F_G can deviate from being perfectly perpendicular to the handle and still cause the desired unstable behaviour. It can deviate up to θ_s in the direction pointing towards the gripper surface in contact with the handle. In the other direction, the force can be up to parallel with the handle. This angle θ_s is a design parameter specific to the constructed surface.

For this design, there is an unstable equilibrium point $F_{u,e}$ at the backside of the surface if F_G is perfectly perpendicular. However, in reality small disturbances and vibrations will cause the gripper to not get stuck on this point.

When the gripper first collides with the handle, it can bounce back as a partially inelastic collision. In order for the aligning mechanism to work, contact between the gripper and handle should be maintained. Thus, the kinetic energy of the gripper should become zero in the least amount of time to limit the number and amplitude of bounces. This bouncing effect is amplified by the reaction force F_R and reduced by the damping of the gripper shaft. As such, it can be minimised by moving the gantry slower (which lowers the cable force F_G and the resulting F_R), or adding additional damping on the gripper shaft to dissipate more energy.

D. Ungrasping Mechanism

The ungrasping procedure is depicted in Fig. 11. If the payload is in the static workspace (Fig. 11a), ungrasping the handle is trivial. The gantry can be positioned straight above the handle. The gripper can then be lowered, releasing the handle from the inner gripping area. Afterwards the gantry is moved away from the handle, such that the gripper can be reeled in and retrieved.

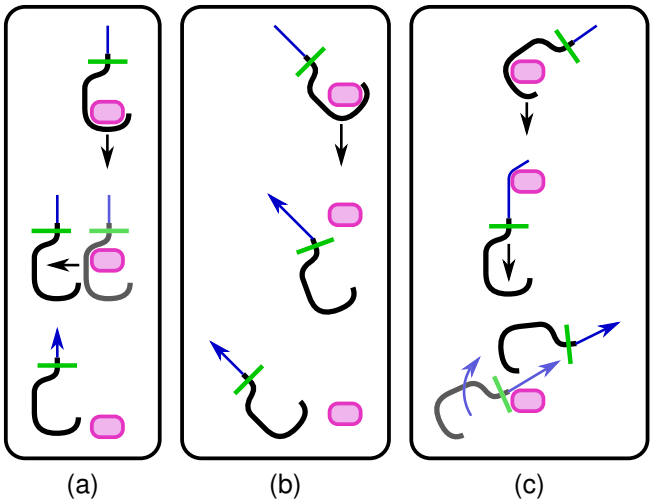

Fig. 11. Side-view of the ungrasping process of the handle. The handle is given in magenta, motions due to cable forces are given with blue arrows, motions due to gravity with black arrows. (a) Ungrasping in the static workspace. (b) Ungrasping with the gripper sliding over the front of the gripper. (c) Ungrasping with the gripper sliding over the back of the gripper.

If the payload is outside of the static workspace, the gantry can no longer be positioned above the handle. Thus, a different tactic is employed: The cable is unwound such that the gripper will slide down until it is entirely below the handle. Depending on the angle of the cable, the gripper will slide along either the front of the gripping area (Fig. 11b), i.e. the rightmost Ⓞ of Fig. 8; or the back of the gripping area (Fig. 11c), i.e. the leftmost Ⓞ, Ⓨ, and the bottom of the tracker. The cable force F_G ensures that the handle remains in contact with Ⓞ or Ⓨ, as explained in Sec. V-C.

For the former, the cable is away from the handle, and the gripper can simply be reeled in without any risk of re-engaging with the handle. For the latter, the cable runs over the top of the handle. Reeling in the gripper in this scenario causes the top of the tracker to touch the bottom of the handle. Due to the flanged shape of the tracker, the cable force will result in a moment on the gripper, which causes it to rotate up and away from the handle. If the cable is retracted fast enough, the gripper will slide and skip over the handle before it is

reoriented in its stable vertical position. Thus, it can be pulled away from the handle without re-engaging with it. In case a different sensing technique is used instead of such a tracker, an additional flange-shaped element could be designed at the top of the gripper.

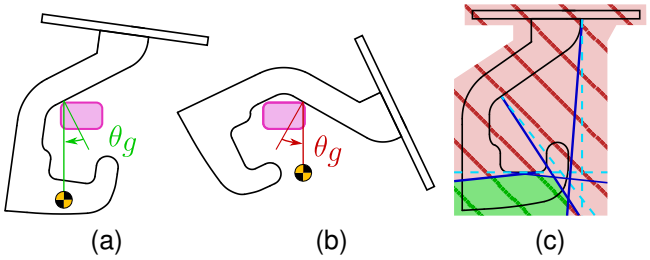

Fig. 12. Influence of the CoG position when ungrasping. (a) Desired sliding away from the handle (given in magenta). (b) Undesired sliding towards the handle. (c) CoG positions with the desired behaviour along every point of the surface (green highlight). CoG positions with the undesired behaviour, at at least one point of the surface (red highlight). Both are in the quasi-static case. Cyan lines are normals of the surface, blue lines reflect the friction angle.

The CoG and the inside surface of the gripper should be designed such that gravity will always cause the gripper to slide away from the handle (Fig. 12a). Otherwise, the gripper could get stuck or slide back to the inner gripping area when the cable is unwound (Fig. 12b). Thus, at every point along the surface, the angle θ_g (between the normal of the surface, and the line connecting the point with the CoG) should point towards the desired sliding direction, away from the handle. This θ_g should be large enough such that it can overcome the friction angle. Figure 12c illustrates positions of the CoG that will achieve the desired sliding behaviour in the quasi-static case, for all points along the inside surface of the gripper. In practise, using a dynamic motion limits the required θ_g.

VI. Task Execution

The task is split up in two sequential parts. First, the crate is grasped while it is positioned stationary on a surface. If a successful grasp is detected, then it is lifted up and shelved. The execution for both parts will be explained and validated separately in following sections.

A. Crate Grasping

The grasping skill process is illustrated in Fig. 13. Both the position of the tracker at the top of the gripper (Fig. 3), and the crate need to be known in the Cartesian world frame. In this work, a direct end-position measurement in the horizontal plane, of both the tracker and the crate, is obtained by the camera image. It should be noted that the orientation of the tracker does not need to be known. The path along which the gripper should approach the handle to align itself is determined as follows: First, the locations of the corners of the crate (•) are identified. These are then used to calculate the middle of both longitudinal crate sides (×). Since the handle is in the middle of the crate, moving the gripper in the direction of the line connecting these two middle points ensures it will approach the handle perpendicularly.

The gripper can deviate from this middle line when it is moving towards the handle (illustrated with the purple area in Fig.13). As long as it collides with the handle, it will be able to grasp it. The potential offset will later be compensated.

Depending on the phase of the execution, the built-in velocity controller of the motor drives, or a simple position controller (constructed as a PID-controller around this velocity controller) is used at the lowest control level of the robot. The exact performance of the used low-level controllers has little impact on the task execution strategy. As such, this will not be discussed in detail. The high-level control implementation is done with the FSM depicted in Fig. 14. It consists of the following states and transitions (the corresponding low-level control output can be deduced from Fig. 17):

1) ***Go-to-start-position***
The gripper starts in a random position and is lifted such that it is above the crate. The gantry moves just outside of the footprint of the crate, close to the middle of one of the long sides of the crates. During this process, the gripper might be swinging wildly. When the gantry is in position, and the gripper is a distance d_s from the crate, state transition ⓪ triggers.
2) ***Damp-vibrations***
The gripper is lowered to the same height of the crate, landing outside of the footprint of the crate. The gantry moves towards the closest middle point (×), a small distance over the crate, such that the gripper will collide with the side of the crate. This creates a horizontal force component which pulls the gripper against the side of the crate, effectively damping all vibrations. ① triggers if the gantry is in position, and the gripper has been stationary for a given amount of time.
3) ***Insert-gripper***
The gripper is first lifted above the crate. When the swing angle is within a certain margin d_a, it is lowered inside of the crate, triggering ②.
4) ***Grasp-handle***
The gantry moves towards the handle in the direction of the furthest middle point (×). Again, the distance is overshot to create a horizontal force component F_G. This force is necessary to make sure the gripper aligns with the handle as explained in section V-B. When the gantry finishes its movement, and the gripper is within a distance d_g of the middle of the handle, ③ triggers. If it is outside of this margin, it signifies that the gripper, for whatever reason, missed the handle. This triggers ④ instead, restarting the grasp procedure.
5) ***Reposition-gantry***
First, the cable is reeled in such that it makes contact with the handle. The motor current is monitored to detect an increase in torque. If the gripper is raised above the crate without triggering this monitor, ⑥ activates. If the monitor does trigger, the gripper is lowered slightly, such that it is still constrained in the direction perpendicular to the handle by ⊖. Then, the gantry is moved directly above the crate handle. A constant distance from Σ is maintained by using (5). If at any time the position of the gripper is more than

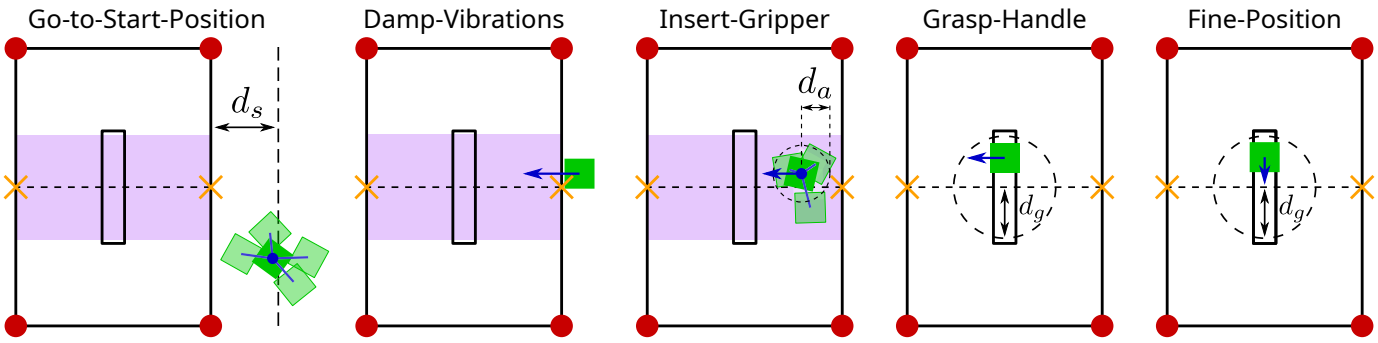

Fig. 13. Top-down view of the FSM execution (Fig. 14) to grasp the crate depicted in Fig 3. The end-effector is represented by a green square, vibrations of the end-effector are depicted with a lighter shade. The cable is given in blue, with arrows depicting the direction of the cable force. The paths along which the gripper can move to successfully make contact with the handle, given the proposed approach, are depicted in purple. The crate corners detected by the image processing are given with ●, the calculated middle points with ×. The *reposition-gantry* and *lift-until-tension* states are not depicted.

d_g from the middle of the handle, it signifies the grasp was lost, and ⑥ triggers. Otherwise, ⑤ triggers when the gantry is above the crate handle.

6) ***Fine-position***
The gripper is moved along the handle towards the middle, using Θ as guides. In order not to excite the flexibility of the cable, a slow, quasi-static gantry speed is used. If the gripper at any point gets stuck on the handle, i.e. it remains stationary while the cable angle increases, the cable is reeled down slightly. When the gripper reaches the middle of the handle and remains stationary, ⑦ triggers.

7) ***Lift-until-tension***
Finally, the gripper is hoisted up until Σ makes contact with the crate, and some cable tension is present such that the gripper does not slip. By monitoring a sudden change in the motor current, the moment when contact is made is detected, triggering ⑧. This indicates a successful grasp, and the process of shelving the payload can start. Again, if the gripper is hoisted above the crate without triggering this monitor, the grasp was lost somewhere during the execution, and ⑨ activates instead.

When these states are referenced in the text, they will be written in *italics*.

If at any point a state takes longer than a given pre-defined time, a generic timeout is given, and the grasp is reattempted from the *go-to-start-position* state.

B. Shelf Insertion

After grasping the payload, it will be positioned outside of the static workspace of the gantry. The use case worked out in this paper is to place the payload inside a shelf. The position inside the shelf is vertically obstructed by the top of the shelf, and is not accessible without a dynamic approach. This corresponds to the most difficult level of the dynamic motions as identified in Sec. I. The other levels could use a similar approach, but with a simpler model than the one used for the shelf insertion.

The shelf insertion process of the payload is depicted in Fig. 15. The payload is first moved quasi-statically above the shelf. Afterwards, energy is injected into the system. Then it is lowered to the height of the shelf, and finally it is inserted

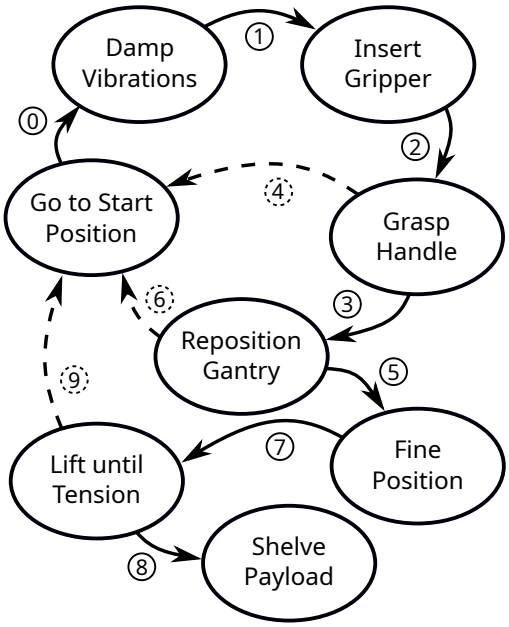

Fig. 14. Finite state machine used for the high-level control of the grasping task. The transitions during nominal execution are given with solid arrows, the transitions that signify an error are given with dashed arrows. For readability, the state transitions from any state to the *go-to-start-position* state, due to a generic timeout error, are not depicted.

using the two-phase pendulum model (Sec. IV-B). During the lowering and the insertion process, the gantry is positioned such that the cable will hit the edge of the shelf at $\theta = 0$. Thus, minimising the required energy of the payload to reach a certain insertion distance, according to (13).

First, the required angle θ_{st} (and thus the required potential energy h_{st}) is calculated by solving (13) given an insertion distance $x_{e,\max}$. Based on θ_{st}, the required swing up angle θ_{sw} before lowering the payload needs to be determined. The difference in energy between these two states is only due to the work done when extending the cable. This work can be calculating with (2b) and (6). Approximating the integral as a discrete sum at every timestep i, over a horizon N gives:

$$h_W = \frac{W}{gm} \approx \frac{1}{g} \sum_{i}^{N} \left(g \cos(\theta_i) + \dot{\theta}_i^2 l_i - \ddot{l}_i \right) \dot{l}_i \Delta t. \qquad (14)$$

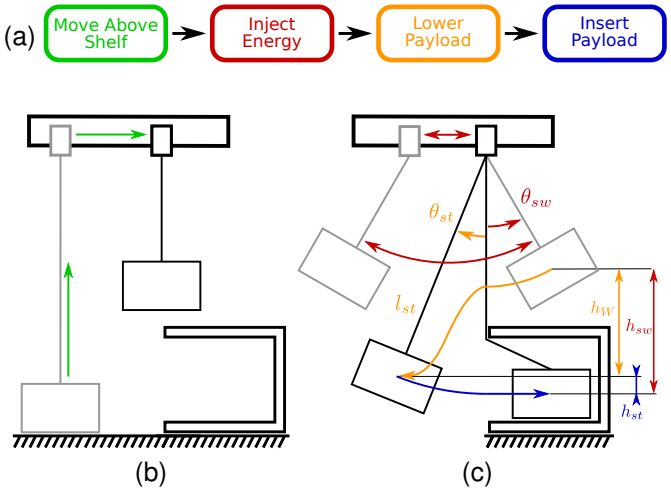

Fig. 15. (a) Different steps of the shelf insertion process. (b) The payload is positioned above the shelf. (c) Energy is first injected in the system by swinging the payload up to θ_{sw}, then the cable is unwound to l_{st}, and finally it is inserted in the shelf.

Dividing W by gm removes the dependency on the mass of the payload, and expresses the work done as a change in maximum potential height h_W. Due to the dependency on both $\dot{\theta}_i$ and θ_i (which are in turn dependent on θ_{sw}), (14) cannot be solved analytically. Thus, θ_{sw} is iteratively solved, starting from an initial guess $\hat{\theta}_{sw}$, by evaluating:

$$h_{st}(\theta_{st}) + h_W(\hat{\theta}_{sw}) - h_{sw}(\hat{\theta}_{sw}) = 0. \tag{15}$$

This results in a non-linear equation in one variable θ_{sw} that can be solved with standard numerical root-finding methods.

Once this value of θ_{sw} is known, energy can be inserted in the system such that this value is reached at the apex of the swing. When $\theta \geq \theta_{sw}$, the payload is lowered to a cable length of l_{st} while the payload is swinging away from the shelf, such that it will not collide with the shelf.

After lowering the payload, the pendulum motion is resumed until $\theta = 0$ is reached. Then a horizontal trajectory, given by (5), is applied when the payload is inside the shelf. The input for this trajectory has to be calculated in advance based on the model, and applied in feedforward, since the view to the tracker is obstructed by the top of the shelf. When this feedforward trajectory (and thus the horizontal movement) is finished, the tension in the hoist is released. This causes the payload to be dropped inside the shelf, and finishes the placement.

VII. Experimental Validation and Discussion

To validate the gripper design, a prototype was manufactured out of 3D-printed PLA.

The experiments were executed by a Beckhoff C6670 industrial computer running Ubuntu 22.04, with an Intel Core i7-9700E processor, and 32GB of RAM. Custom C++ code was written to implement the methodology. The control loop of the robot operates at 500Hz with the EtherCAT protocol.

In the following experiments, the horizontal position of the crate was measured with the camera during online execution. Depending on the required accuracy, the vertical distance from the gantry to the crate can be estimated based on the detected size of the crate and the (known) tracker size in the image frame. In case better accuracy is required, additional sensing can be utilised (e.g. a 3D camera, or a laser distance sensor). This estimation is however deemed out of scope for the contents of this paper. The vertical distance was instead measured manually offline.

The cyclic output data of the used motor drives did not provide the information to perform a thorough energy consumption analysis. However, if different drives were to be used, a similar methodology as in [22], [23] could be applied.

A video showcasing the execution of all the experiments discussed in this section can be found in [37].

A. Nominal Grasping Experiment

To test the gripper during nominal use, the crate depicted in Fig. 3 was grasped multiple times. For practical reasons, the crate was always positioned in roughly the same position, such that it was within the static workspace of the gantry. The developed methodology is invariant to this position, since the gantry could move to any starting position. The orientation of the crate in relation to the gantry was varied. Trials with eight different crate orientations where performed (from 0° to 157.5°, with 22.5° intervals). For each orientation the crate was grasped from both sides, three times each. Due to the symmetry of the crate, this can be treated as doubling the number of orientations to 16 (from 0° to 337.5°). Thus, a wide range of starting poses were represented.

Before initialising the grasping sequence, the gantry was moved manually such that the gripper would swing around randomly. This mimics the potential sway that would be present from finishing a previous task, or moving from a previous position. The execution is shown in Figure 16. The corresponding position and velocity of the gantry (expressed in the frame defined in Fig. 16a, with its origin in the middle of the handle, and the Y-axis along the length of the handle), and the cable length is given in Fig. 17.

In 47 out of the 48 trials, the crate was grasped successfully from the first attempt. In the remaining trial, the gripper was swinging too wildly during the *insert-gripper* state for state transition ② to trigger in time, instead it prompted a timeout, and the grasp was reattempted. During this second iteration the grasp was performed successfully as well.

A boxplot showing the cumulative elapsed time for each state is given in Fig. 18. The execution time of the *go-to-start-position* state is not taken into account during the analysis, since this solely depends on the distance of the starting position of the gantry to the crate. The total time it took to complete the grasp, starting from the *go-to-start-position*, varied from 18.4s to 35.35s (with a median of 20.9s).

The largest variation in the execution time occurred during the *fine-positioning* state. This is due to the slow quasi-static gantry velocity that is used during this state, combined with the variation of the gripper's position along the handle at the start of the state (which is caused mainly whether the gripper had to rotate significantly to reach the correct orientation during the *grasp-handle* state). This variation could be significantly reduced by taking the dynamic behaviour of the gripper into

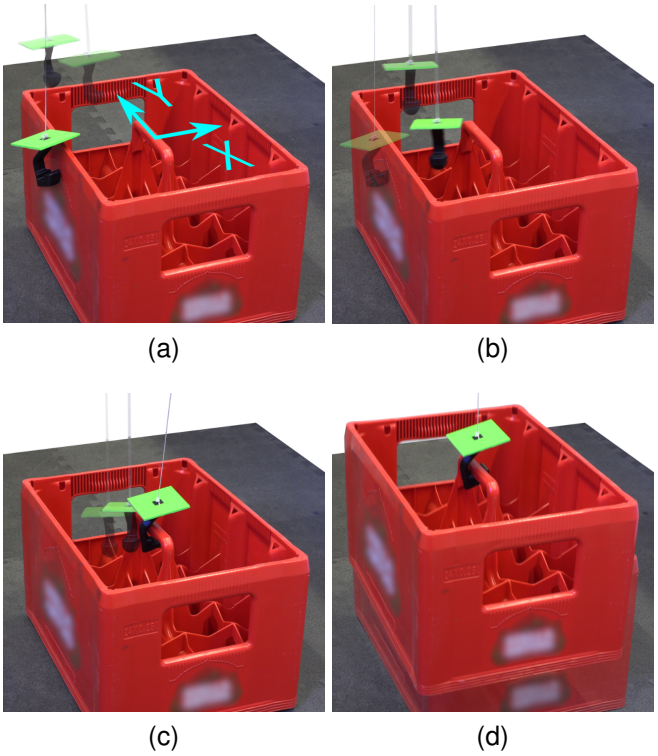

Fig. 16. The grasping experiment [37]. (a) Going from *go-to-start-position* to *damp-vibrations*. (b) *Insert-gripper*. (c) Mechanically aligning the gripper during *grasp-handle*. (d) *Lift-until-tension*.

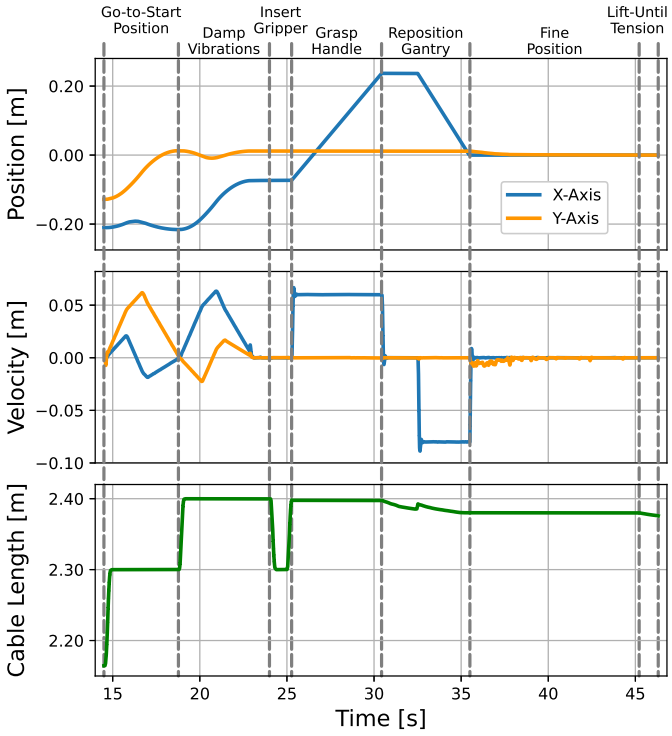

Fig. 17. The gantry's position and velocity, and the cable length for one of the trials of the grasping experiment (Fig. 16). The coordinates are expressed in the frame depicted in Fig. 16a.

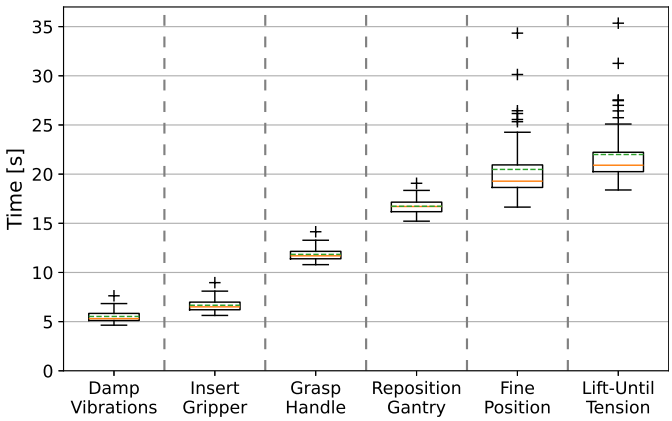

Fig. 18. Boxplot of the cumulative time it took to finish executing each state of the grasping procedure. The median is given with a full line, the mean with a dashed line, and outliers with +. The time it takes to perform the *go-to-start-position* state is omitted. Only the time durations of the successful iterations are considered.

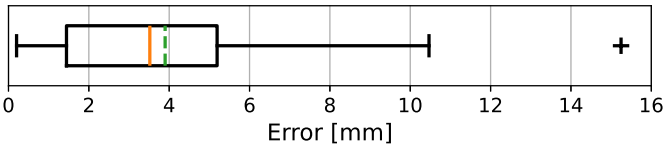

Fig. 19. Boxplot of the final distance of the gripper from the middle of the crate's handle, along the direction of the handle. The median is given with a full line, the mean with a dashed line, and outliers with +.

account, since this would allow for a much higher gantry velocity.

Figure 19 shows a boxplot indicating the distance of the gripper from the middle of the handle, along the direction of the handle (Y-axis of Fig. 16a). This is the distance at the end of the *lift-until-tension* state, as detected by the camera. It showcases a median distance of ±3.5mm, with 75% of trials below 5.2mm. The single outlier corresponds to ±15.2mm. The error was lower at the end of the *fine-positioning* state, but the gripper could still slide slightly during the lifting state due to the convex shape of the handle (which is ergonomically designed for humans). Thus, increasing the error when finishing the grasp.

The camera was at a distance of 2.4m from the top of the crate, resulting in a resolution of ±2mm. This is well around the range of the perceived errors. As such it can be concluded that the perceived error is nearly completely compensated in the control execution. The limiting factor for securing a grasp in the middle of the handle is thus the accuracy of the handle detection, which falls outside of the scope of this work.

These successful results also show that the used quasi-static model for the gripper aligning is valid for the investigated use case (assumption 1. of Sec. V).

B. Grasping Error Monitors

Additional experiments where performed to test the detection of faulty grasps at the different stages of the execution. Each of the following experiments was repeated three times, each with the crate in a different orientation across trials.

For the first experiment, the gripper was thrown such that it swung wildly before the gantry reached the start position. This allowed the gripper to rest against the small side of the crate

during the *damp-vibrations* state, instead of the long side. This caused the gripper to swing along the direction of the handle (Y-axis of Fig. 16a) when it was inserted in the crate, failing to catch the handle during the *grasp-handle* state.

For the second experiment, a plate was put in front of the handle, such that the gripper could not hook around the handle. Thus, preventing the handle to be properly grasped during the *reposition-gantry* state, causing the gripper to be lifted above the handle. For the second grasping attempt after triggering the error monitor, this plate was removed.

For the last experiment, the same plate was used, however during the *reposition-gantry* state, the gripper was manually held into place, to simulate the gripper getting stuck on something else than the handle. During the *lift-tension* state, the gripper was lifted above the handle without grasping it. Again, the plate was removed after the first attempt.

In all experiments, the fail-safe monitors triggered correctly (respectively state transitions ④, ⑥, and ⑨ of Fig. 14), detecting a faulty grasp. The second iteration of the grasping procedure was always able to successfully perform a proper grasp. This showcases the ability to detect and recover from a faulty grasp during various stages of the execution.

C. Ungrasping Experiment

Ungrasping the payload when the handle is still in the static workspace was not explicitly validated since this is trivial. However, an experiment was performed to validate the ungrasping mechanism when the payload is outside of the static workspace (Fig. 20). A small steel weight was glued to the bottom of the gripper to lower the CoG such that it is in the green-highlighted region of Fig. 12c. The gripper started in a grasping state around the handle of the crate. The crate was positioned such that the cable of the gripper is angled at $\pm 50°$ with respect to the vertical. The cable was unwound 15cm, before being reeled in at a velocity of $0.4\frac{\mathrm{m}}{\mathrm{s}}$. Both of these inputs are executed in a feedforward manner. Five trials were performed with the gripper positioned as illustrated in Fig. 11b. 10 trials were performed with the gripper as illustrated in Fig. 11c (as shown in Fig. 20).

In all 15 trials, the handle was successfully ungrasped on the first attempt. This shows that the ungrasping mechanism is a reliable method to retrieve the gripper, regardless of its position or orientation, with minimal control from the robot. Thus, it illustrates the potential of the ungrasping mechanism to assist in automating pick-and-place tasks.

D. Shelf Insertion

The system was set up to perform shelf insertions with a desired insertion distance $x_{e,\max,d}$ of 15cm, 20cm, and 25cm. This was performed three times for each $x_{e,\max,d}$. A table frame was used to simulate the shelf. The table top was removed such that the camera could still view the gripper when it was underneath the table. This data was only used to validate the models in post-processing, not to provide sensory feedback to the robot during the task execution. Snapshots for one of the trials of these experiments are depicted in Fig. 21.

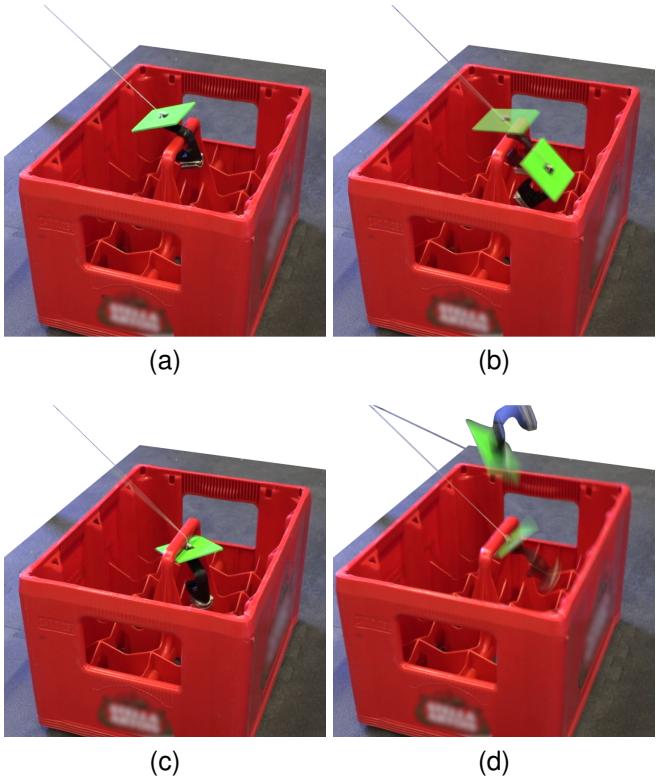

Fig. 20. The ungrasping experiment [37]. (a) Starting position. (b) Lowering the gripper below the handle. (c) Top of the gripper making contact with the bottom of the handle. (d) Skipping the gripper over the handle to recover it.

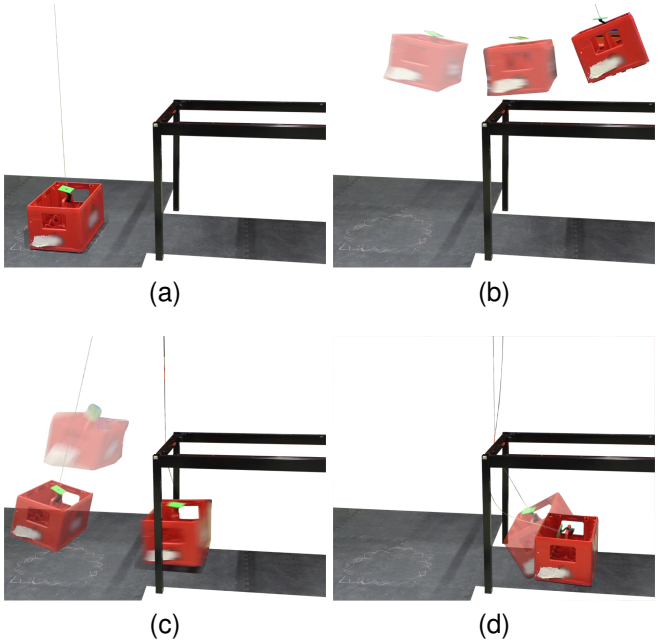

Fig. 21. The shelf insertion experiment [37]. (a) Starting position. (b) Injecting energy by swinging the crate up. (c) Unwinding the cable to l_{st}. (d) Horizontal movement underneath the shelf, and placement of the crate

The starting energy necessary to reach θ_{sw} is injected by moving the gantry in resonance with the payload using visual feedback. When the angular velocity of the gripper changes sign, the gantry is moved with high acceleration between two

predefined positions. With this method the exact calculated value of θ_{sw} will not be reached due to the discrete increase of the maximum swing angle in the swing-up process. While more elaborate methods such as MPC could be used, this is not the focus of this work.

A generic trapezoidal velocity trajectory with a ramp-up/down acceleration of $8\frac{\mathrm{m}}{\mathrm{s}^2}$ and a maximum velocity of $2\frac{\mathrm{m}}{\mathrm{s}}$ (satisfying (3)) is applied to the hoist to unwind the cable to l_{st} during the lowering phase.

Figure 22 compares the experimental result with a simulated trajectory based on the two-phase pendulum model (Sec. IV-B). It illustrates one of the trials for $x_{e,\max,d} = 20\text{cm}$, $l_{sw} = 1.55\text{m}$, and $l_{st} = 2.31\text{m}$. During the swing-up state, $\theta_{sw} = 17.84°$ was reached, with the calculated desired value being $\theta_{sw,d} = 17.72°$. Due to tracking issues of the hoist, after the lowering of the payload the final cable length was only $l_{st} = 2.29\text{m}$. These actual values were always copied for the simulations that are used for comparison.

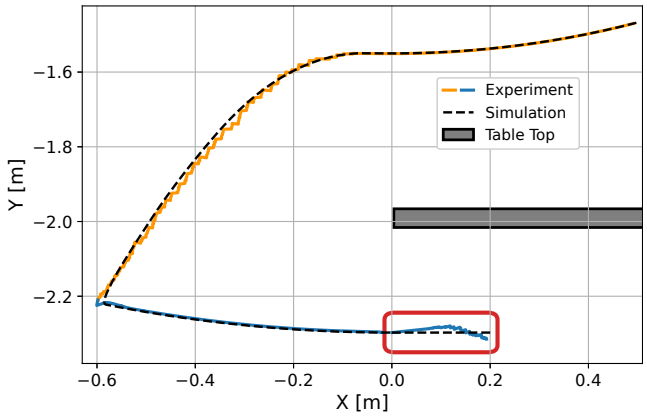

Fig. 22. Side-view comparison of the trajectory of the end-effector for an experimentally performed shelf insertion for $x_{e,\max,d} = 20\text{cm}$, and the corresponding model simulation. The cable anchor is positioned at the origin. The colours of the experimental trajectory correspond to the stages as in Fig. 15 (the swing-up of the payload is not depicted). The table top is depicted with the grey rectangle. The insertion is highlighted in red. During this section, the hoist cable is in contact with, and pivots around, the edge of the table.

Figure 22 shows a good match between the actual experiment and the simulation. A similar path is followed during the lowering of the payload, resulting in a similar value of θ_{st}. The energy losses, expressed as a change in maximum potential height h_W, are depicted in Fig. 23 for both the experimental and simulated trajectories. The error is in general a couple millimetres, and remains under 5mm for every trial. This indicates that (14) is able to sufficiently capture the energy loss. Similar results leading to the same conclusions were found for the other trials of the experiment.

A close-up of the insertion section (red highlight in Fig. 22) is illustrated in Fig. 24, for all of the trajectories. While the trajectories overall move horizontally, they do exhibit some vertical error with a maximum deviation of 2cm in both directions. The error has a similar course across the different trials. The end-effector moves upwards first, because the cable does not unwind fast enough, which results in a larger angle θ_2. Afterwards, the cable extends too fast, since the end-

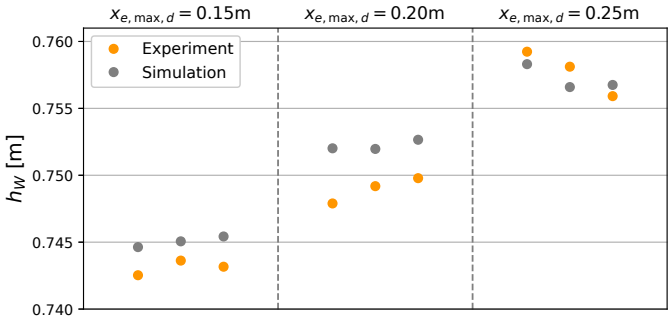

Fig. 23. Loss of maximum potential height, h_W, during the lowering of the payload (orange section of Fig. 22) for both the experimental results and the model simulations.

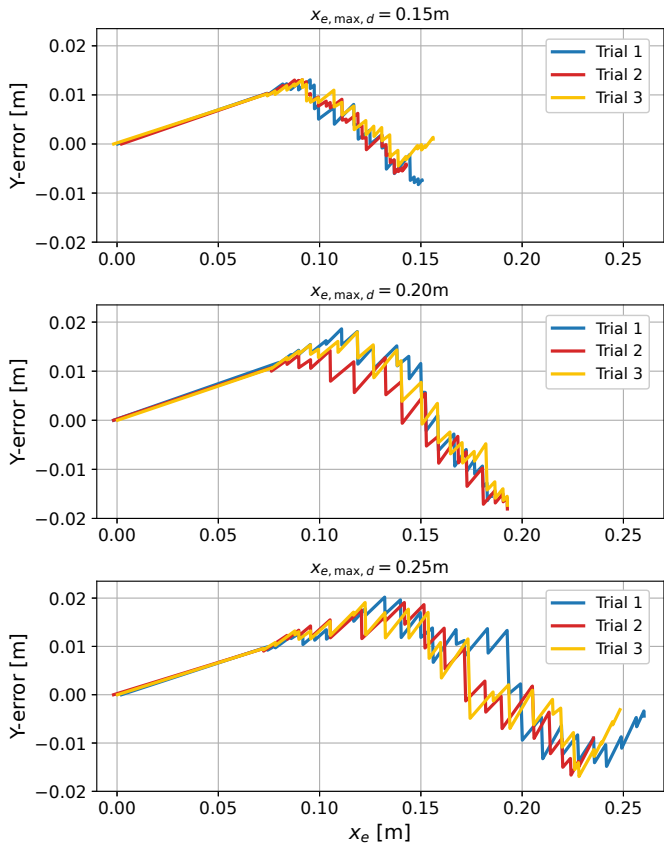

Fig. 24. Close-up of the red highlight in Fig 22. It depicts the vertical error between the experimental trajectories and the desired horizontal trajectory along the insertion distance x_e. The initial straight line until $x_e \approx 0.07\text{m}$ is caused due to the visual obstruction of the tracker by the table frame.

effector slowed down more than anticipated, causing it to move downwards.

The origin of these errors is due to the imperfect tracking of the feedforward velocity commands $\dot{l}_2$ by the hoist motor, as can be seen in Fig. 25. Due to the relative short cable length l_2 during the pendulum motion underneath the table, small errors in the tracking of the desired length cause relatively larger errors in both θ_2 and $\dot{\theta}_2$ (compared to a long cable length). This results in even larger errors of $\dot{l}_2$ conform (5), and consequently a non-perfect horizontal trajectory. Thus, it can be concluded that assumption 5. of the pendulum model (Sec. IV) is not valid for this use case. Other potential error

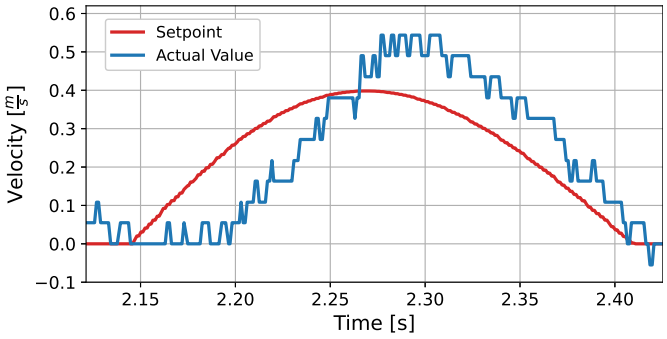

Fig. 25. Actual velocity and setpoint of $\dot{l}_2$ during the horizontal trajectory underneath the table. Values correspond to the trajectory displayed in Fig. 22

TABLE I
FINAL INSERTION DISTANCE FOR THE EXPERIMENTS, COMPARED TO THE CORRESPONDING SIMULATIONS.

Desired $x_{e,max,d}$	Trial no.	Experiment [cm]	Simulation [cm]
15cm	1	14.9	16,0
	2	14.3	15,0
	3	15.6	15,8
20cm	1	18,5	19,6
	2	19,3	20,8
	3	19,3	20,6
25cm	1	26,0	26,4
	2	23,7	24,7
	3	24,8	25,3

and disturbance sources are:

- Unmodelled energy losses (e.g. friction when sliding the cable over the edge of the table, cable elongation).
- Manually measured geometric errors.
- A non-constant hoist drum radius due to the cable overlapping with itself.
- Measurement errors of the tracker by the vision system.

Nevertheless, in all cases the final insertion distance $x_{e,\max}$ is within 1.5cm of the desired insertion distance $x_{e,\max,d}$. This is well within the required accuracy for the application. An overview of all the simulated and experimental insertion distances x_e is given in Table I.

VIII. CONCLUSION

This paper showed that even while using a gantry system that is underactuated in the three rotational DoF, by co-developing different aspects of the mechatronic design, it can still perform certain pick-and-place tasks that depend on these rotational DoF.

This shortcoming could be overcome, even when only simple low-level controllers were used, by developing a passive gripper with a predictable mechanical interaction behaviour, and using the inherent compliance of the cable. The relevant design parameters were identified, and the corresponding trade-offs for the task execution were given.

The effectiveness of a passive gripper, designed for a specific handle, was validated with a grasping task. In the nominal case, the grasping task could be reliably executed. It only failed once on the first attempt out of 48 trials. Monitors that track the nominal behaviour were able to detect this failure, prompting the task to be retried, which succeeded on the second attempt. The median total execution time, starting from the end of the *go-to-start-position* state, was 20.9s. The largest variation was caused by the quasi-static gantry movement during the *fine-position* state. Incorporating the dynamics of the gripper during this motion could significantly reduce this variation. Separate tests were performed that simulate failures at different states of the execution. Again, this was always successfully detected by the monitors, and the task execution could recover from this, succeeding on the second attempt. This showcases the resilience and robustness of the high level controller to system disturbances. To validate the ungrasping mechanism of the gripper, an experiment was executed were the crate was ungrasped when it was positioned outside of the static workspace. A simply control sequence was used were the hoist cable was first unwound, and then reeled in. In all 15 trials, the gripper was successfully retrieved by the robot. This shows the effectiveness of the ungrasping mechanism, regardless of the position and orientation of the gripper.

It was also shown that by making use of dynamic, time-dependent trajectories, obstructed positions that are unreachable with traditional control methods for such systems, could be reached. This was illustrated with a shelf insertion task. The trajectories were modelled by a combination of two variable-length pendulum models, which only dependent on kinematic parameters. Comparisons between experimental and simulation results showed a high similarity during the first phase of the motion, when the cable length is long. However, the horizontal motion inside the shelf was less accurate due to the unmodelled tracking delay of the motor. Still, the final insertion distance was in all cases close to the desired distance, and well within the requirements for the handled applications. This shows the potential of the developed solution.

It should also be noted that only a single 2D camera is necessary as external sensing to perform both of these tasks.

IX. FUTURE WORK

Future work includes developing a second robot agent whose task is to assist with the stages of the execution where accuracy is needed, such as: precise positioning of the payload (by pushing the payload after it has been dropped); creating a physical brace for the crane to swing the payload against; or helping with (un)grasping the end-effector from the handle. The hardware should be backdrivable such that it can withstand the impact from colliding with the (potentially swinging) payload. This second robot could also assist with sensing when the vision of the main robot is obstructed, or to provide better sensing near the region of interest. This could be achieved by e.g. a depth camera, or an eye-in-hand camera. Thus, the task and robot requirements would be separated between respectively a strong-, and a precise robot, resulting in two complementary heterogeneous designs.

Currently, the robot is not capable of grasping a payload from inside a shelf. A possible approach (complementary to a second robot system) could be to 'throw' the gripper over the payload, and slowly reel in the hoist, in order to 'fish' for the handle. In case the gripper catches the handle, this would

be detectable with a spike in the motor current. If the gripper misses the handle, it will be retracted outside of the shelf, and another attempt can be made.

Yet another path to explore would be to add more cables in parallel to the gripper in order to (selectively) increase the controllability. Additionally, it could be used to increase the stiffness in some well chosen directions.

ACKNOWLEDGEMENTS

All authors gratefully acknowledge the financial support by Research Foundation-Flanders (FWO) project ELYSA (S001821N), and the European Union Horizon Europe research and innovation program under grant agreement No 101058589 (AI-PRISM).

REFERENCES

[1] "Silka installation 2016," YouTube, uploaded by Laurie Van Belle, 6 April 2017, last accessed on 24 March 2025, https://www.youtube.com/watch?v=RDa-CBaU2Ws&ab_channel=LaurieVanBelle.

[2] N. Hogan, "Impedance Control: An Approach to Manipulation," in *1984 American Control Conference*, San Diego, California, USA, pp. 304-313 1984.

[3] Fanuc Robot Range Overview, last accessed 23 April 2025, https://www.fanuc.eu/robot-range

[4] "Truck Unloading (2/20/2021)," YouTube, uploaded by Cody Peaster, 21 February 2011, last accessed on 24 March 2025, https://www.youtube.com/watch?v=dFPw5IbZoLs&t=381s&ab_channel=CodyPeaster.

[5] H. Lee, "Modeling and Control of a Three-Dimensional Overhead Crane," *Journal of Dynamical Systems, Measurement, and Control*, vol. 120, no.4, pp 471-476, 1998.

[6] A. Benhidjeb, G. L. Gissinger, "Fuzzy control of an overhead crane performance comparison with classic control," *Control Engineering Practice*, vol. 3, no. 12, pp. 1687-1696, 1995.

[7] D. Chwa, "Sliding-Mode-Control-Based Robust Finite-Time Antisway Tracking Control of 3-D Overhead Cranes," *IEEE Transactions on Industrial Electronics*, vol. 64, no. 8, pp. 6775-6784, Aug. 2017.

[8] N. C. Singer, W.P. Seering, "Preshaping command inputs to reduce system vibration," *Journal of Dynamical Systems, Measurement, and Control*, vol 112., no. 1, pp. 76-82, March 1990.

[9] W. Singhose, N. Singer, W. Seering, "Comparison of Command Shaping Methods for Reducing Residual Vibration," in *Proceedings of the Third European Control Conference*, Rome, Italy, pp. 1126-1131, 1995.

[10] Z. N. Masoud, K. A. Alhazza, "Frequency-Modulation Input Shaping Control of Double-Pendulum Overhead Cranes," *Journal of Dynamical Systems, Measurement, and Control*, vol. 136, no. 2, pp. 1-11, March 2014.

[11] E. Maleki, W. Singhose, S. S. Gürleyük, "Increasing Crane Payload Swing by Shaping Human Operator Commands," *IEEE Transactions on Human-Machine Systems*, vol. 44, no. 1, pp. 106-114, Feb. 2014.

[12] L. Barbazza, D. Zanotto, G. Rosati and S. K. Agrawal, "Design and Optimal Control of an Underactuated Cable-Driven Micro–Macro Robot," *IEEE Robotics and Automation Letters*, vol. 2, no. 2, pp. 896-903, April 2017.

[13] Mason, M., "Manipulator Grasping and Pushing Operations," Ph.D. dissertation, Dept. of Elec. Eng and Comp. Sc., M.I.T. Cambridge, USA, 1982.

[14] Eppner C., Deimel R., Álvarez-Ruiz J., Maertens M., Brock O, "Exploitation of environmental constraints in human and robotic grasping," *Int. J. Robotics Research*, vol. 34, no. 7, pp. 1021-1038, 2015.

[15] L.Van den Broeck, M. Diehl and J. Swevers, "A Model Predictive Control Approach for Time Optimal Point-to-point Motion Control," *Mechatronics*, vol. 21, no 7, pp. 1203–1212, 2011.

[16] M. Vukov, W. Van Loock, B. Houska, H. J. Ferreau, J. Swevers and M. Diehl, "Experimental validation of nonlinear MPC on an overhead crane using automatic code generation," in *American Control Conference*, Montreal, QC, Canada, pp. 6264-6269, 2012.

[17] N. van Duijkeren, R. Verschueren, G. Pipeleers, M. Diehl and J. Swevers, "Path-following NMPC for serial-link robot manipulators using a path-parametric system reformulation," in *European Control Conference*, Aalborg, Denmark, pp. 477-482, 2016.

[18] A. Steinhauser and J. Swevers, "An Efficient Iterative Learning Approach to Time-Optimal Path Tracking for Industrial Robots," *IEEE Transactions on Industrial Informatics*, vol. 14, no. 11, pp. 5200-5207, Nov. 2018.

[19] K. Paes, W. Dewulf, K. Vander Elst, K. Kellens, P. Slaets, "Energy efficient trajectories for an industrial ABB robot," *Procedia CIRP*, vol. 15, pp. 105–110, 2014.

[20] P. Boscariol and D. Richiedei, "Spline-based energy-optimal trajectory planning for functionally redundant robots," in *2018 14th IEEE/ASME International Conference on Mechatronic and Embedded Systems and Applications (MESA)*, Oulu, Finland, pp. 1-6, 2018

[21] M. Pellicciari, G. Berselli, F. Leali, A. Vergnano, "A method for reducing the energy consumption of pick-and-place industrial robots," *Mechatronics*, vol. 23, no.3, pp. 326–334, 2013.

[22] B. Deroo, E. Aertbeliën, W. Decré., H. Bruyninckx, "Energy-Efficient Control of Cable Robots Exploiting Natural Dynamics and Task Knowledge," in *6th Int. Conf. on Cable-Driven Parallel Robots*, Nantes, France, pp 184-196, 2023.

[23] B. Deroo, B. Pousett, E. Aertbeliën, W. Decré and H. Bruyninckx, "The Need for Task-Specific Execution in Robot Manipulation: Skill Design for Energy-Efficient Control," in *2023 IEEE 19th International Conference on Automation Science and Engineering (CASE)*, Auckland, New Zealand, pp. 1-7, 2023.

[24] Lynch K, Mason M. "Dynamic Nonprehensile Manipulation: Controllability, Planning, and Experiments," *The International Journal of Robotics Research*, vol. 18, no. 1, pp. 64-92, 1999.

[25] H. Miyashita, T. Yamawaki and M. Yashima, "Learning control method for throwing an object more accurately with one degree of freedom robot," in *2010 IEEE/ASME International Conference on Advanced Intelligent Mechatronics* Montreal, QC, Canada, pp. 397-402, 2010.

[26] Haddadin, S., Huber, F., Albu-Schäffer, A, "Optimal control for exploiting the natural dynamics of variable stiffness robots," in *2012 Proc. IEEE Int. Conf. on Robotics and Automation*, Saint Paul, MN, USA, pp. 3347-3354, 2012.

[27] H. Arisumi, K. Yokoi and K. Komoriya, "Kendama game by casting manipulator," in *2005 IEEE/RSJ International Conference on Intelligent Robots and Systems*, Edmonton, AB, Canada, pp. 3187-3194, 2005.

[28] H. Arisumi, K. Yokoi and K. Komoriya, "Casting Manipulation—Midair Control of a Gripper by Impulsive Force," *IEEE Transactions on Robotics*, vol. 24, no. 2, pp. 402-415, April 2008.

[29] D. Cunningham and H. H. Asada, "The Winch-Bot: A cable-suspended, under-actuated robot utilizing parametric self-excitation," in *2009 IEEE International Conference on Robotics and Automation*, Kobe, Japan, pp. 1844-1850, 2009.

[30] D. P. Cunningham and H. H. Asada, "Continuous path tracing by a cable-suspended, under-actuated robot: The Winch-Bot," in *2010 IEEE International Conference on Robotics and Automation*, Anchorage, AK, USA, pp. 1255-1260, 2010.

[31] L. Scalera, A. Gasparetto and D. Zanotto, "Design and Experimental Validation of a 3-DOF Underactuated Pendulum-Like Robot," *IEEE/ASME Transactions on Mechatronics*, vol. 25, no. 1, pp. 217-228, Feb. 2020.

[32] D. Zanotto, G. Rosati and S. K. Agrawal, "Modeling and Control of a 3-DOF pendulum-like manipulator," in *2011 IEEE International Conference on Robotics and Automation*, Shanghai, China, 2011, pp. 3964-3969.

[33] N. Zoso and C. Gosselin, "Point-to-point motion planning of a parallel 3-dof underactuated cable-suspended robot," in *2012 IEEE International Conference on Robotics and Automation*, Saint Paul, MN, USA, 2012, pp. 2325-2330.

[34] Flat linear robot, Igus, last accessed on 27 November 2024, https://www.igus.be/product/21023?C=BE&L=nl&artNr=DLE-FG-0005-01.

[35] Dyneema, last accessed on 16 April 2025, https://www.dyneema.com/.

[36] L. Scalera, P. Gallina, S. Seriani and A. Gasparetto, "Cable-Based Robotic Crane (CBRC): Design and Implementation of Overhead Traveling Cranes Based on Variable Radius Drums," *IEEE Transactions on Robotics*, vol. 34, no. 2, pp. 474-485, April 2018.

[37] "Mechatronic Design and Control of a Robotised Crane," YouTube, uploaded by Robotics Research Group, KU Leuven, 11 December 2025, last accessed on 11 December 2025, https://www.youtube.com/watch?v=9TPT5XezT2M



Boris Deroo received the M.Sc. degree in Mechanical Engineering from KU Leuven, Leuven, Belgium, in 2020. He is currently finishing his Ph.D. at the Department of Mechanical Engineering at KU Leuven.
His research interest include robot manipulation exploiting their natural dynamics, control strategies that utilise the mechanical compliance of the system and interactions with the environment, hardware that can be passively controlled, and tactics to improve the energy-efficiency during robot operation.



Erwin Aertbeliën received the M.Sc. and Ph.D. degrees in Mechanical Engineering from KU Leuven, Leuven, Belgium, in 1995 and 2008 respectively. He is currently a Research Expert at KU Leuven, specialising in robot task specification and control. He is the developer and originator of the constraint-based task specification formalism known as eTaSL. His research interests include all forms of human–robot collaboration, including lower-limb and upper-limb exoskeletons, co-manipulation with robot manipulators, teleoperation using brain interfaces, and the capturing and modelling of craftsmanship skills. In addition, he has a research activity in quantitative analysis of spasticity and related phenomena.



Wilm Decré received the M.Sc. and Ph.D. degrees in Mechanical Engineering from KU Leuven, Leuven, Belgium in 2006 and 2011 respectively. He is currently an associate professor at KU Leuven, specialising in programming and control of smart and high-performance machines, vehicles and robotic systems.
He received over ten academic and industry research prizes including a KUKA Innovation Award and an IEEE Robotics and Automation Letters (RA-L) Best Paper Award. He co-founded KU Leuven spin-off SoundTalks. His research interests include sensor- and optimization-based control of robot systems, numerical optimization algorithms and applications, learning and optimal control and estimation, and real-time and embedded software design.



Herman Bruyninckx obtained the Masters degrees in Mathematics (1984), Computer Science (1987) and Mechatronics (1988), and the Ph.D. degree in Mechanical Engineering (1995) all from KU Leuven, Leuven, Belgium. He is currently a full-time Full Professor at KU Leuven, and part time at the Eindhoven University of Technology.
His research focus in both places is on the composability of the most advanced, knowledge driven algorithms for the dynamics of motion control of complex robotics applications, with distributed sensor processing and resource monitoring. The complementary objectives are to realise such systems with the least amount of resource costs, with ”good enough” quality, and with full explainability.

He held visiting research positions at the University of Pennsylvania, Philadelphia, Stanford University, and the Kungl Tekniska Hogskolan in Stockholm. Between 2007 and 2015, he was leading the European academic community, first as Coordinator of the European Robotics Research Network EURON, and later as Vice-President Research of euRobotics He was the Principal Investigator in about two dozen European research projects on robotics, with a focus in the recent years on the systems and software engineering aspects of multi-agent robotic skills.